

# Engineered Ovalbumin Nanoparticles for Cancer Immunotherapy

Nahal Habibi, Stephanie Christau, Lukasz J. Ochyl, Zixing Fan, Alireza Hassani Najafabadi, Matthias Kuehnhammer, Mengwen Zhang, Matthew Helgeson, Regine von Klitzing, James J. Moon, and Joerg Lahann\*

Ovalbumin (OVA) is a protein antigen that is widely used for eliciting cellular and humoral immune responses in cancer immunotherapy. As an alternative to solute OVA, engineering approach is developed herein towards protein nanoparticles (pNPs) based on reactive electrospaying. The resulting pNPs are comprised of polymerized OVA, where individual OVA molecules are chemically linked via poly(ethylene glycol) (PEG) units. Controlling the PEG/OVA ratio allows for fine-tuning of critical physical properties, such as particle size, elasticity, and, at the molecular level, mesh size. As the PEG/OVA ratio decreased, OVA pNPs are more effectively processed by dendritic cells, resulting in higher OT-I CD8<sup>+</sup> cells proliferation *in vitro*. Moreover, pNPs with lower PEG/OVA ratios elicit enhanced lymphatic drainage *in vivo* and increased uptake by lymph node macrophages, dendritic cells, and B cells, while 500 nm OVA pNPs show poor draining lymph nodes delivery. In addition, pNPs with lower PEG/OVA ratios result in higher anti-OVA antibody titers *in vivo*, suggesting improved humoral immune responses. Importantly, OVA pNPs result in significantly increased median survival relative to solute OVA antigen in a mouse model of B16F10-OVA melanoma. This work demonstrates that precisely engineered OVA pNPs can improve the overall anti-tumor response compared to solute antigen.

their efficacy in clinical trials has been disappointing, mostly due to inefficient delivery of antigen and adjuvants to draining lymph nodes, resulting in immune tolerance and cytotoxic T lymphocyte fratricide.<sup>[3]</sup> On the other hand, high levels of vaccine have been linked to T cell sequestration at the vaccination site, resulting in systemic T cell exhaustion and deletion.<sup>[4]</sup> Nanoparticles have been utilized to enhance the therapeutic outcome of cancer immunotherapies in the context of subunit antigens, dendritic cell-based vaccines, immune checkpoint inhibitors/blockade, adoptive T-cell therapy<sup>[5]</sup> and immunoenhancing agents for *in situ* vaccination.<sup>[6]</sup> Cancer vaccine strategies that aims to improve early steps of antigen delivery and processing can be also beneficial to patients who lack the sufficient pre-existing anti-tumor T cells.<sup>[5]</sup> Nanoparticle-based delivery platforms hold the potential to improve vaccine immunogenicity<sup>[7]</sup> due to increased antigen stability, sustained release, site-specific delivery, and improved circulation and biodistribution of the antigens.<sup>[1,8,9]</sup> Parameters such as nanoparticle size,<sup>[10]</sup> shape,<sup>[11]</sup> charge,<sup>[12]</sup> and administration route<sup>[13]</sup> are known to affect the immune response, but the mechanism behind cross-presentation and cross-priming of CD8<sup>+</sup> T cells remains an active area of research.<sup>[14]</sup> Typically, antigens have been either encapsulated in the bulk of nanoparticles for

In cancer immunotherapy, eliciting potent and specific immune responses against advanced tumors remains a major challenge.<sup>[1]</sup> Peptide-based cancer vaccines (subunit vaccines) have been extensively studied in the past, because they have significant advantages (such as safety and ease of manufacturing) over attenuated, inactivated, or biosynthetic vaccines.<sup>[2]</sup> However,

and biodistribution of the antigens.<sup>[1,8,9]</sup> Parameters such as nanoparticle size,<sup>[10]</sup> shape,<sup>[11]</sup> charge,<sup>[12]</sup> and administration route<sup>[13]</sup> are known to affect the immune response, but the mechanism behind cross-presentation and cross-priming of CD8<sup>+</sup> T cells remains an active area of research.<sup>[14]</sup> Typically, antigens have been either encapsulated in the bulk of nanoparticles for


N. Habibi, Dr. S. Christau, Z. Fan, Prof. J. Lahann  
Department of Chemical Engineering  
University of Michigan  
Ann Arbor, MI 48109, USA  
E-mail: lahann@umich.edu

N. Habibi, Dr. S. Christau, Dr. L. J. Ochyl, A. Hassani Najafabadi,  
Prof. J. J. Moon, Prof. J. Lahann  
Biointerfaces Institute  
University of Michigan  
Ann Arbor, MI 48109, USA

Dr. L. J. Ochyl, A. Hassani Najafabadi, Prof. J. J. Moon  
Department of Pharmaceutical Sciences  
University of Michigan  
Ann Arbor, MI 48109, USA

M. Kuehnhammer, Prof. R. von Klitzing  
Department of Physics  
Technische Universitaet Darmstadt  
Darmstadt 64289, Germany

Dr. M. Zhang, Prof. M. Helgeson  
Department of Chemical Engineering  
University of California Santa Barbara  
Santa Barbara, CA 93106, USA

 The ORCID identification number(s) for the author(s) of this article can be found under <https://doi.org/10.1002/adtp.202000100>

DOI: 10.1002/adtp.202000100

subsequent release or were presented on the surface of nanoparticles. Polymer nanoparticles made of natural or synthetic polymers, such as chitosan or poly(lactic-co-glycolic acid) (PLGA), have been extensively studied for vaccine encapsulation.<sup>[15,16,71]</sup> Other examples of antigen-encapsulating nanomaterials include lipid nanocapsules,<sup>[7f,h]</sup> polyelectrolyte capsules comprised of peptide antigens and adjuvants made by the layer-by-layer technique,<sup>[7m]</sup> or nanoparticles comprised of antigen or adjuvant molecules linked to lipophilic albumin-binding tails.<sup>[7k]</sup> In contrast, antigen conjugation to the surface of nanoparticles<sup>[17]</sup> has been suggested to be superior compared to antigen encapsulation for two main reasons: Firstly, the nanoparticles themselves were found to trigger inflammatory immune responses when encountered by antigen-presenting cells (APCs).<sup>[18]</sup> Secondly, antigens presented on the nanoparticle surface can more effectively interact with surface receptors of APCs, which appears to enhance crosstalk between the innate and adaptive immune system.<sup>[19]</sup> As an alternative, virus-like particles (VLPs) or protein nanoparticles (pNPs) have been pursued in some instances.<sup>[7b,20]</sup> VLPs are biomimetic engineered particles, which mirror viruses in their structural properties. The main concern of VLPs is the risk of inducing anti-carrier antibody production. This could potentially limit their clinical translation, because repeated dosing could lead to neutralization or reactive toxicities in patients.<sup>[21]</sup> In addition, off-target immune response can be caused by the competition between the carrier antigen and the target antigen.<sup>[22]</sup> Using pNPs comprised of the actual antigen as the main structural unit eliminates the need for a separate nanoparticle carrier.<sup>[23]</sup> If the entire particle, or its majority, is comprised of antigen, pNPs have the potential for enhancing dendritic cell surface receptor engagement, prolonging tissue persistence, sustaining antigen activity and minimizing off-target material delivery.<sup>[22]</sup> In the past, proteins have been assembled into particles through structurally ordered assembly, unstructured hydrophobic assembly and electrostatic assembly.<sup>[22]</sup> However, these protein assemblies driven by fusion and sequence modification are more likely affected by antigenic variability and the loss of their capacity to self-assemble and preserve antigen recognition.<sup>[22]</sup> Compared to fusion and sequence modification, chemical conjugation to proteins, lipids or polymers, promises versatility and broader applicability to a wider spectrum of antigens, but requires multiple processing steps.<sup>[22]</sup> For example, crosslinked peptide nanoclusters were fabricated for delivery of oncofetal antigen by desolvation and were stabilized through disulfide bonds.<sup>[23f]</sup> However, changes to the primary structure of the protein, such as addition of cysteine to the C-terminus of the peptide, was necessary to ensure successful crosslinking.

Another method of nanoparticle fabrication is electrospaying, which involves liquid atomization through electrical forces.<sup>[24]</sup> Electrospaying has been employed in biomedical research for fabrication of different types of nanoparticles based on natural materials, such as elastin-like polypeptide nanoparticles<sup>[25]</sup> or insulin particles.<sup>[26]</sup> Electrospaying is a one-step process, which can be applied to a range of proteins and protein mixtures without significantly increasing the engineering effort.<sup>[24]</sup> Another potential advantage of electrospaying is its proven scalability, which makes it a valuable method of particle fabrication in industrial applications.<sup>[27]</sup> In electrospaying, the liquid is transported through a metal capillary, which is connected to a con-

ductive substrate. The characteristic Taylor cone is formed at the tip of the capillary after applying high voltage; nanoparticles are formed after evaporation of the solvent and collected on a conductive substrate.<sup>[24]</sup>

Here, we report a novel synthetic route toward pNPs comprised of polymerized ovalbumin (OVA) linked by poly(ethylene glycol) (PEG) units based on reactive electrospaying. This scalable particle fabrication technique limits denaturation of proteins as confirmed by circular dichroism spectroscopy.<sup>[28]</sup> Reactive electrospaying can be extended to fabricate bicompartamental protein nanoparticles;<sup>[29]</sup> therefore, fabrication of multicompartamental nanoparticles where each compartment is made of a different antigen can be feasible with this method which is hard-to-achieve otherwise. Conceptually, this approach has the potential to reduce competing anti-carrier responses, because the target antigen becomes the actual structural building block in pNPs. This novel type of pNPs ensures presentation of dense arrays of antigen that should be readily recognizable by APCs. In pNPs comprised of polymerized OVA, antigen presentation is critically influenced by the crosslinker:protein ratio. Specifically, we have evaluated four types of polymerized OVA pNPs with various PEG: OVA ratios in terms of their uptake by dendritic cells, T cell activation, lymphatic drainage, antibody production, and anti-tumor efficacy.

OVA pNPs were prepared using reactive electrospaying, as shown in **Figure 1A**. To synthesize OVA pNPs, OVA was dissolved in water/ethylene glycol (7.5 w/v%). The OVA solution was mixed with the amine-reactive crosslinker NHS-PEG-NHS at variable ratios. During reactive electrospaying, we employed a solvent mixture comprised of water and ethylene glycol (80:20 vol%) and used NHS-PEG-NHS with molecular weight of 2 kDa. Under these conditions, the PEG units form amide-bonds with amino groups in the antigen, such as OVA's lysine residues, resulting in stable, polymerized OVA pNPs. To ensure completion of the reaction, OVA pNPs were stored at 37 °C for 7 days prior to collection. To adjust the network structure of OVA pNPs, we varied the PEG/OVA ratio as follows: 10% to 30% and 50% (w/w%). Electrospaying resulted in pNPs of 200–300 nm in their fully hydrated state (**Figure 1F**). We found parameters, such as protein concentration, solvent viscosity and solvent dielectric constant, can be adjusted to control the size and network structure in pNPs. To increase the size of hydrated OVA pNPs to 500 nm, the ratio of water-to-ethylene glycol was decreased to 40:60 (vol%), which effectively decreases the overall dielectric constant of the solvent system and increases nanoparticle size.<sup>[32]</sup> However, additional optimization was required to obtain 500 nm OVA pNPs. First, the PEG/OVA ratio was decreased to 5% (w/w). Second, the molecular weight of the PEG crosslinker was increased from 2 to 20 kDa. Through these modifications, we were able to reliably prepare hydrated OVA pNPs with size of 500 nm, as confirmed by dynamic light scattering.

**Figure 1B–E** show SEM images of the different OVA pNPs as collected on the counter electrode. The pNPs were dispersed in PBS buffer, and their zeta potential and size were measured using ELS and DLS. The zeta potentials among four types of OVA pNPs were not statistically significant different (**Table S3**, Supporting Information). The stability of OVA pNPs was confirmed using DLS measurements over a time period of 36 days. (see **Figure S2** in the Supporting Information).

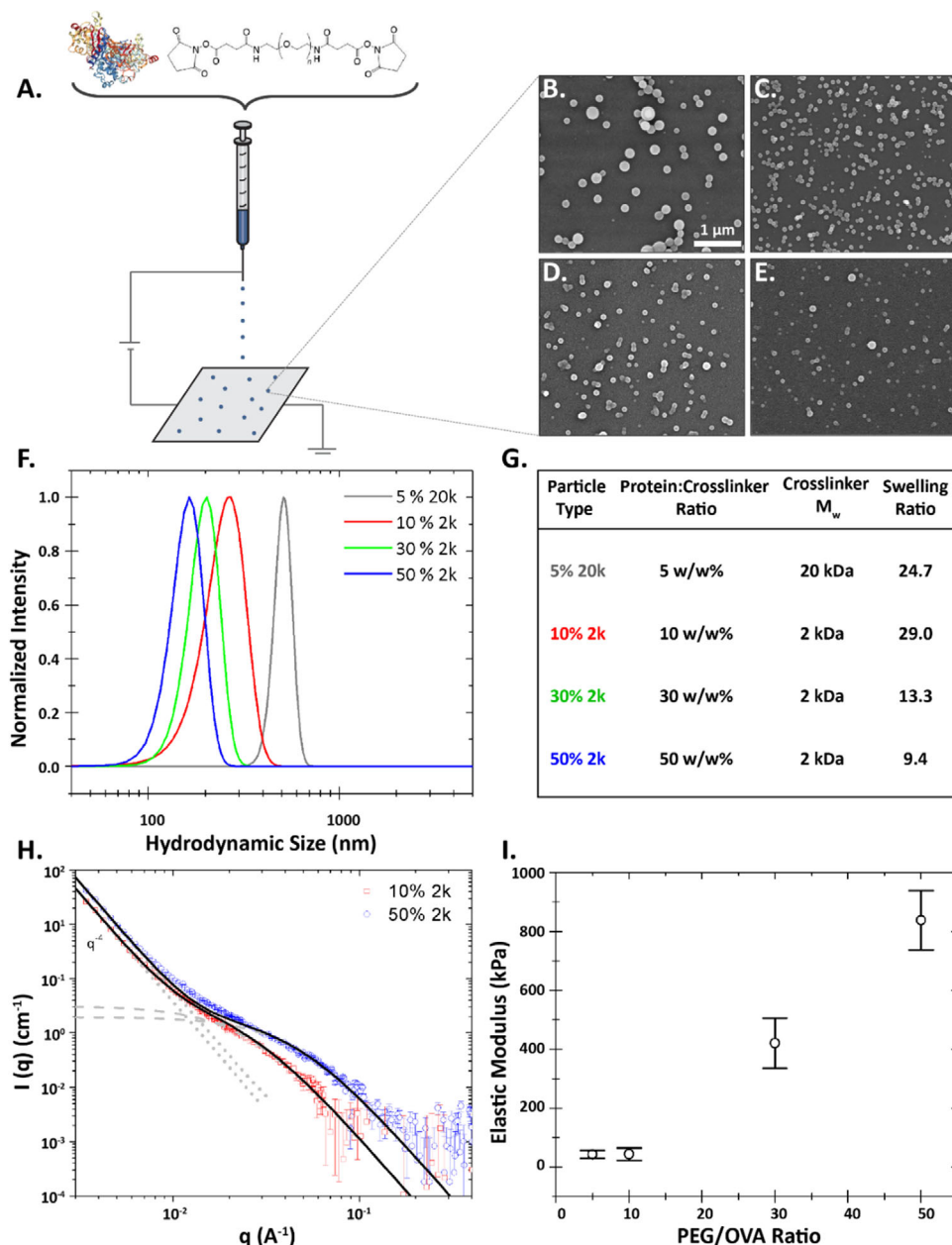


**Figure 1.** Preparation and characterization of four types of engineered OVA pNPs via reactive electro spraying: A) Setup for electro spraying used for preparation of engineered OVA pNPs. SEM images of OVA pNPs with B) 5 w/w% 20 kDa crosslinker, C) 10 w/w% 2 kDa crosslinker, D) 30 w/w% 2 kDa crosslinker, and E) 50 w/w% 2 kDa crosslinker. F) The size of hydrated pNPs was measured using DLS after NP collection and dispersion in PBS buffer. G) shows a table with parameters/conditions for electro spraying of the OVA pNPs. H) SANS data and fits for OVA pNPs with 10% and 50% PEG/OVA ratio. OVA pNPs were dispersed in  $\text{D}_2\text{O}$  at  $2 \text{ mg mL}^{-1}$ . Data were fitted using the Debye-Anderson-Brumberger (DAB) model (see main text for more information). I) Young's modulus as a function of the pNP PEG/OVA ratio. Data were obtained by fitting the force-distance profiles (see Figure S1 in the Supporting Information) obtained from AFM measurements using the Hertz model for a conical indenter.

The size of hydrated nanoparticles characteristically increased with lower PEG/OVA ratio (Figure 1F). The swelling of the particles with respect to their SEM dry size was estimated using<sup>[33]</sup>

$$\text{Swelling ratio} = \frac{V_{\text{swollen}}}{V_{\text{dry}}} \quad (1)$$

where  $d_{\text{DLS}}$  and  $d_{\text{SEM}}$  are the nanoparticle diameters obtained from DLS and SEM (see Table S1 in the Supporting Information for DLS and SEM size data) that were used to calculate  $V_{\text{swollen}}$  and  $V_{\text{dry}}$ , respectively, assuming a spherical geometry for nanoparticles.

OVA pNPs with PEG/OVA ratios of 5%, 10%, 30%, and 50% showed swelling ratios of 24.7, 29, 13.3, and 9.4, respectively.

These differences in the swelling behavior suggest substantial differences in the mesh sizes of the protein gels that the pNPs are comprised of. The dependency of pNP swelling on crosslinker amount indicates that our reactive electrospinning procedure, in fact, does yield particles with different mesh size. However, we aimed at quantifying the mesh size more accurately using small-angle neutron scattering to evaluate the network density of polymerized pNPs.

We conducted SANS measurements of two representative OVA pNPs, 10% and 50% PEG/OVA NPs dispersed in D<sub>2</sub>O (2 mg mL<sup>-1</sup>). We expected that the scattering from the hydrated protein network resembles the scattering from heterogeneous synthetic polymer hydrogels,<sup>[34]</sup> which can be modeled as a disordered two-phase system with a protein-rich network phase and a protein-poor polymer phase. Accordingly, the scattering curves were fitted to a combined Porod model<sup>[35]</sup> and the Debye-Anderson-Brumberger (DAB) model<sup>[36]</sup> (solid black lines in Figure 1H) according to

$$I(q) = \frac{8\pi\Phi(1-\Phi)(\Delta\rho)^2\xi^3}{(1+(q\xi)^2)^2} + \frac{A}{q^4} \quad (2)$$

where  $A$  is a coefficient that determines the relative magnitude of Porod scattering. The DAB model (first term in Equation (2)) describes scattering from the concentration correlations between the protein-rich phase with volume fraction  $\Phi$  and scattering length density contrast  $\Delta\rho$  with the surrounding fluid that is randomly distributed into domains of average spacing  $\xi$ . The Porod model (second term in Equation (2)) represents scattering from smooth interfaces between the protein-rich and protein-poor domains.

Equation (2) provides fits of the observed SANS spectra from the two samples. At low  $q$ -values, we observe a  $q^{-4}$  dependence of the scattering data, consistent with scattering from a smooth interface. At moderate  $q$ -values, the length scale  $\xi$  is apparent as a shoulder in the scattering curve. It should be noted that the overall fit for 50% PEG/OVA pNPs is poor in the region where the Porod and the DAB model contributions are of similar magnitude ( $q \approx 0.01\text{--}0.02 \text{ \AA}^{-1}$ ). The explanation for this lies in the interference between the Porod scattering from the interfaces of the protein-rich domains and the DAB scattering from polymer chains inside the domains. This is not accounted for in the model and would likely show up in the mid  $q$ -range, where the model gives a poor fit.

We found that the DAB scale factor ( $8\pi\Phi(1-\Phi)(\Delta\rho)^2$ ) increases four-fold as the PEG/OVA ratio increased from 10% to 50%, confirming the densification of the protein network as the degree of crosslinking increases. Furthermore,  $\xi$  decreased nearly two-fold as the PEG/OVA ratio increased from 10% to 50% (Table 1), thus revealing a more finely divided structure with increasing PEG/OVA ratio. Together, these results suggest that the protein network becomes denser and more finely heterogeneous with increasing PEG/OVA ratio, consistent with a more porous but smaller mesh structure at higher crosslink density.

Since the ability for the uptake of pNPs by cells might be affected by the mechanical properties of the pNPs, we measured the elastic moduli of the OVA pNPs. We conducted AFM indentation measurements to obtain the elastic moduli for polymer-

**Table 1.** Fitting parameters from DAB model.

	10% PEG/OVA	50% PEG/OVA
Porod scale factor, $A$	$3.70 \times 10^{-9} \pm 2.99 \times 10^{-13}$	$5.92 \times 10^{-9} \pm 1.02 \times 10^{-13}$
DAB scale factor, $8\pi\Phi(1-\Phi)(\Delta\rho)^2$	$4.92 \times 10^{-6} \pm 1.32 \times 10^{-7}$	$1.95 \times 10^{-5} \pm 1.60 \times 10^{-7}$
Correlation length, $\xi$ (nm)	$3.98 \pm 0.12$	$2.15 \pm 0.01$

ized OVA pNPs (Figure 1I; see the Supporting Information for force-indentation profiles, Figure S1, Supporting Information). All AFM force measurements were conducted at 37 °C to mimic cellular uptake experimental conditions. Elastic ( $E$ ) moduli were extracted from the experimental force-indentation profiles by fitting the profiles using the Hertz model for a conical indenter according to

$$F = \frac{2E \tan\theta}{\pi(1-\nu^2)} \delta^2 \quad (3)$$

where  $F$  is the indentation force,  $\delta$  is the indentation,  $\theta$  is the half-opening angle of the indenter,  $E$  is the  $E$  modulus of the NPs, and  $\nu$  is the Poisson ratio of the NPs.<sup>[37]</sup> A value of  $\nu = 0.5$  was used to fit the profiles using Equation (3).<sup>[38]</sup> The Hertz model assumes that the nanoparticles exhibit a uniform  $E$  modulus. It can be applied even for heterogeneous nanoparticles such as our OVA pNPs, as the length scale over which the probe deforms the pNPs is large relative to the size of the density heterogeneities. Our results show that the  $E$  modulus increases with increasing PEG/OVA ratio. This dependency of crosslinker density and  $E$  modulus has been previously observed<sup>[39]</sup> and was associated with increasing stiffness of the OVA pNPs with increasing PEG/OVA ratio. In our study, the increase in  $E$  modulus was directly correlated to the increase in PEG/OVA ratio, as expected for rubber-like materials such as polymer hydrogels.<sup>[40]</sup> The increase in stiffness coincides well with the decrease in correlation length from SANS (Table 1) and the decrease in swelling ability (Figure 1G).

The uptake of engineered OVA pNPs by bone marrow-derived dendritic cells (BMDCs) was evaluated quantitatively by flow cytometry (Figure 2A) and further visualized by confocal microscopy (Figure 2B–E) using AlexaFluor 647-labeled OVA pNPs. The fluorescence intensity of OVA NPs (10  $\mu\text{g mL}^{-1}$ ) was quantified using a plate reader; we found no significant differences in fluorescence intensity between the different nanoparticle groups (see Table S2 in the Supporting Information). To investigate the interaction between OVA pNPs and BMDCs, confocal microscopy was used. BMDCs were incubated with AlexaFluor 647-labeled OVA pNPs with different PEG/OVA ratio for 24 h at 37 °C. The actin filaments were stained with AlexaFluor 488-Phalloidin and the nucleus was stained with DAPI. As shown in Figure 2B–E, OVA pNPs of different PEG/OVA ratio were successfully internalized by BMDCs allowing for intracellular antigen delivery to BMDCs. As seen in the confocal images, pNPs with higher PEG/OVA ratio showed reduced uptake. To quantify the uptake of OVA pNPs by BMDCs, flow cytometry was used. OVA pNPs were incubated with BMDCs for 24 h at a concentration of 10  $\mu\text{g mL}^{-1}$ . Cellular uptake was quantified using flow



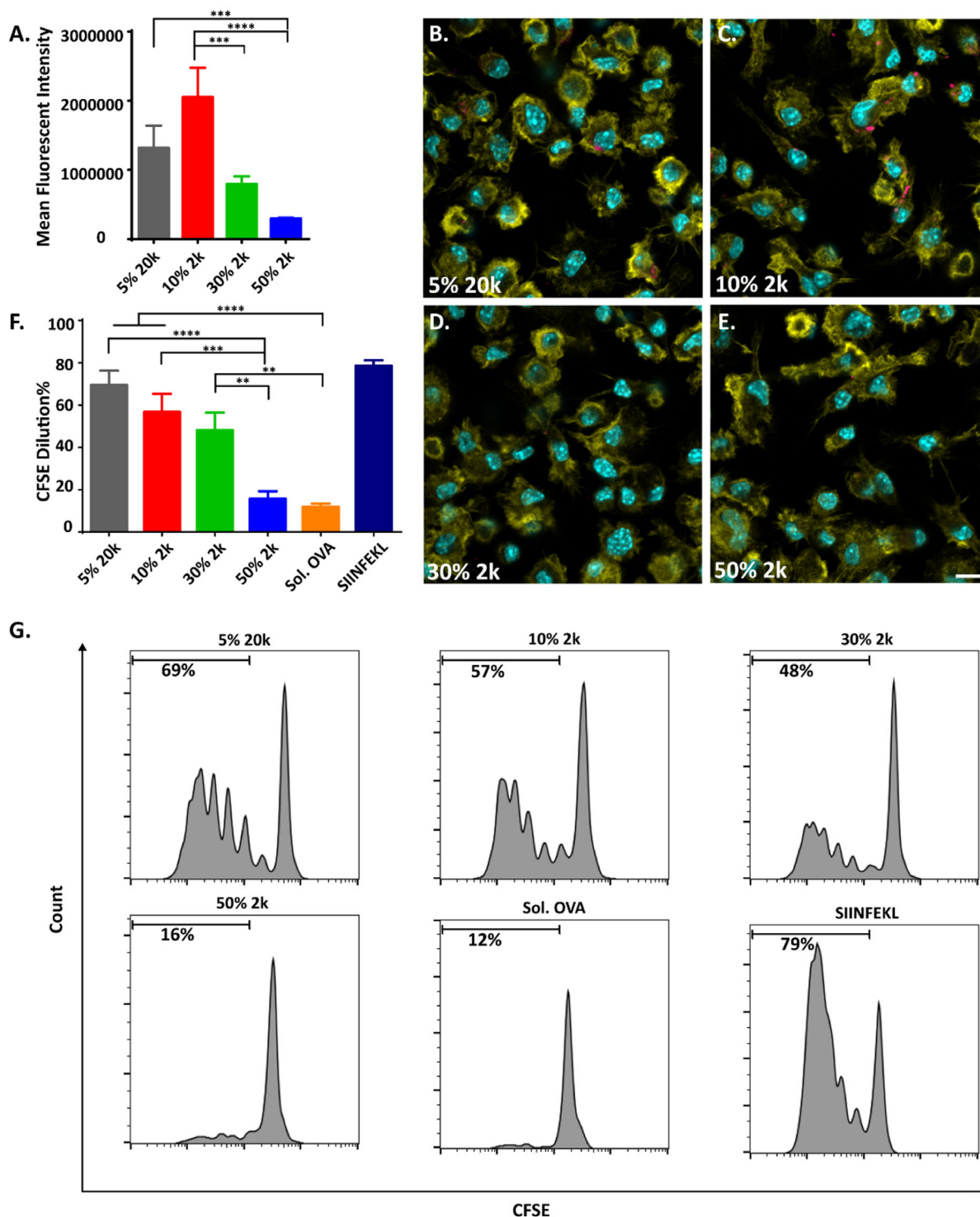


**Figure 2.** In vitro Cell Uptake of fluorescently labeled OVA pNPs by BMDCs: A) Quantitative uptake data (MFI values) were obtained by flow cytometry. The data represent the mean  $\pm$  SEM using triplicates. B–E) Uptake was further visualized by confocal microscopy. BMDCs were incubated with OVA pNPs (magenta) at  $10 \mu\text{g mL}^{-1}$  for 24 h. The actin filaments were stained with AlexaFluor 488-Phalloidin (yellow) and the nucleus was stained with DAPI (blue). Scale bar is  $10 \mu\text{m}$ . For flow cytometry, BMDCs were stained for DC marker CD11c+ using anti-CD11c+ PE-Cy7; they were also stained with DAPI. For confocal microscopy, actin was stained with phalloidin488 and nuclei were stained with DAPI. OVA pNP-treated BMDCs induce proliferation of OT-I CD8+ cells: F) Percentage of proliferated OT-I CD8+ cells after co-culture with BMDCs incubated with  $10 \mu\text{g mL}^{-1}$  OVA pNPs (5% 20k XL, 10% 2k XL, 30% 2k XL, 50% 2k XL). The data represent the mean  $\pm$  SEM from triplicates of three experiments. G) Representative flow cytometry histograms of (F). All shown data were analyzed by one-way ANOVA, followed by Tukey's post-test. A  $P$ -value of  $<0.05$  was considered statistically significant (\* $P < 0.05$ , \*\* $P < 0.01$ , \*\*\* $P < 0.001$ ; \*\*\*\* $P < 0.0001$ );  $P$ -values of  $>0.05$  were considered not significant (ns).

cytometry by comparing the mean fluorescence intensity (MFI) values (see Figures S4–S7, Supporting Information). Our data show that there is a difference in the MFI values for OVA pNPs with different crosslinking density. MFI values were increased for pNPs with lower PEG/OVA ratio (10%), which correlated with higher cellular uptake, compared to the other groups. Cells incubated with pNPs with a 10% PEG/OVA ratio showed 6.9-fold greater MFI than those exposed to pNPs comprised of 50% PEG/OVA ( $P < 0.0001$ ). However, MFI values for cells incubated with pNPs with 5% and 10% PEG/OVA ratios were not statistically different ( $P > 0.05$ ). It has been shown previously that the elasticity of nanoparticles affected cellular uptake: Nanoparticles with Young's moduli between 30 and 140 kPa showed the highest uptake by RAW 264.7 macrophages, while softer (<30 kPa) or harder (>140 kPa) NPs showed reduced uptake.<sup>[41]</sup> In our case, pNPs with PEG/OVA ratios of 5% and 10%, which had intermediate elasticity as indicated by E moduli of  $E = 43$  kPa, were associated with the highest levels of cellular uptake.

Eliciting an effective immune response requires delivery of OVA to APCs, such as dendritic cells (DCs). DCs digest OVA through a process called cross-presentation, which results in the activation and proliferation of CD8+ T cells. Thus, the ability of OVA pNP-treated BMDCs to promote antigen cross-presentation and induce antigen-specific proliferation of OT-I CD8+ cells were evaluated using a CFSE dilution assay (Figure 2F,G). CFSE dilution is proportional to the proliferation of OT-I CD8+ cells. Therefore, BMDCs were first incubated with OVA pNPs or soluble OVA (control) at  $10 \mu\text{g mL}^{-1}$  for 24 h. BMDCs were then co-cultured with CFSE-labeled naïve OT-I CD8+ T cells, which recognize the OVA-derived epitope SIINFEKL presented in the context of MHC-I H2K<sup>b</sup>. After 72 h of co-culture, the population of proliferated CD8+ T cells was assessed using flow cytometry. We found that proliferation was affected by the PEG/OVA ratios of the pNPs. The OVA pNPs with PEG/OVA ratio of 5% showed 4.4-fold ( $P < 0.0001$ ) higher proliferation rates than pNPs with a 50% PEG/OVA ratio. Similarly, pNPs with PEG/OVA ratio of 10% and 30% showed 3.6-fold ( $P < 0.001$ ) and 3.1-fold ( $P < 0.01$ ) higher proliferation rates than pNPs comprised of 50% PEG/OVA, respectively. Cross-priming and proliferation of the OT-I CD8+ cells were significantly enhanced for OVA pNPs with 5% ( $P < 0.0001$ ), 10% ( $P < 0.0001$ ), and 30% ( $P < 0.01$ ) PEG/OVA ratios as compared to soluble OVA (Figure 2F). While all pNP groups outperformed soluble OVA, 5% and 10% PEG/OVA pNPs were most efficient in promoting antigen cross-presentation and proliferation of OT-I CD8+ cells. This result suggests 1) greater uptake of 5% and 10% PEG/OVA pNPs by BMDCs and 2) facilitated the processing of OVA pNPs by BMDCs due to lower crosslinking density and larger size of 5 and 10% PEG/OVA pNPs. There is some evidence that larger particles can direct antigen to the class I antigen presentation pathway more efficiently,<sup>[42]</sup> which might explain the higher proliferation values for 5% PEG/OVA pNPs (500 nm vs 200 nm). Once internalized by BMDCs, smaller particles are shuttled more rapidly to an acidic environment than larger ones,<sup>[14a]</sup> which can lead to fast and unregulated degradation and inefficient cross-presentation.<sup>[14a]</sup> Larger particles remain longer in a neutral environment, thus preserving the antigens for more efficient cross-presentation.<sup>[14a]</sup> Our results indicate that the PEG/OVA ratio is an important parameter for enhancing proliferation of CD8+

T cells, lower PEG/OVA ratios resulting in higher proliferation rates.

Our next aim was to investigate the in vivo performance of the pNPs by evaluating their ability to induce humoral immune responses in mice. Following the prime-boost vaccine regimen shown in Figure 3A, we injected C57BL/6 mice subcutaneously at the tail base with OVA pNPs of varying PEG/OVA ratio (10%, 30%, 50%) and size (200 nm, 500 nm) or soluble OVA (10  $\mu\text{g}$  OVA per 100  $\mu\text{L}$  dose), co-administered with CpG (15  $\mu\text{g}$  per dose). Boost immunization was performed on day 21 after primary immunization. Anti-OVA serum IgG responses were measured on days 20 and 42 using an ELISA assay. Compared to soluble OVA, pNPs with a 10% PEG/OVA ratio elicited 49.4-fold increase in anti-OVA serum IgG titers in prime ( $P < 0.0001$ ) and 9.1-fold increase in boost immunization ( $P < 0.05$ ), respectively. In addition, anti-OVA serum IgG titers induced after prime immunization with pNPs of 30% and 50% PEG/OVA ratios exhibited 39.9-fold ( $P < 0.0001$ ) and 26.5-fold ( $P < 0.01$ ) increase compared to soluble OVA, respectively. Among the pNPs groups, 10% PEG/OVA ratio pNPs outperformed pNPs comprised of 50% PEG/OVA, as indicated by a 1.9-fold increase in anti-OVA serum IgG titers after prime immunization ( $P < 0.01$ ). Our results show that 2 doses of OVA pNPs administered in a prime-boost regimen elicited stronger humoral immune responses than the equivalent doses and regimen of soluble OVA (Figure 3B,C). While the larger, 5% PEG/OVA pNPs showed stronger CD8+ T cell responses in vitro, the same particles elicited a weaker humoral immune response in vivo (comparable to soluble OVA). Because the elasticity of 5% and 10% PEG/OVA pNPs was similar, the weaker humoral immune response of 5% PEG/OVA pNPs can be attributed to their larger size (500 nm). Larger pNPs may have limited lymphatic drainage due to extended tissue persistence at the injection site.

Next, we evaluated the pNPs targeting of the draining lymph nodes using AlexaFluor 647-labeled pNPs. OVA pNPs of varying PEG/OVA ratio (10%, 30%, 50%) and size (200 nm, 500 nm) were injected subcutaneously at the tail base of C57BL/6 mice (10  $\mu\text{g}$  OVA per 100  $\mu\text{L}$  dose). The inguinal draining lymph nodes were harvested 48 h after injection. We prepared single-cell suspensions from the draining lymph nodes and analyzed pNPs uptake among the different populations of antigen-presenting cells (dendritic cells, macrophages and B cells) using flow cytometry by comparing the MFI values of the cells. We found that the MFI values of F4/80+ macrophages, B220+ B cells and CD11c+ DCs (Figure 3D–F) increased with decreasing PEG/OVA ratio for the smaller (200 nm) pNPs with 10%, 30% and 50% PEG/OVA ratio. 50% PEG/OVA pNPs did not show any significant difference compared to soluble OVA. However, 10% PEG/OVA pNPs were delivered more efficiently to F4/80+ macrophages ( $P < 0.05$ ), B220+ B cells ( $P < 0.01$ ) and CD11c+ DCs ( $P < 0.005$ ) compared to 50% PEG/OVA pNPs. Specifically, the antigen delivery to B220+ B cells by 10% PEG/OVA pNPs, even at short time point, was increased compared to 50% ( $P < 0.01$ ), 5% PEG/OVA pNPs ( $P < 0.01$ ) and soluble OVA ( $P < 0.05$ ), which correlated well with the trend of induction of anti-OVA serum IgG titers measured by ELISA. The MFI values of cells with larger (500 nm) 5% PEG/OVA pNPs was significantly lower than 10% PEG/OVA pNPs, indicating that the pNPs were not delivered to draining lymph nodes efficiently due to their larger size. In the past, many

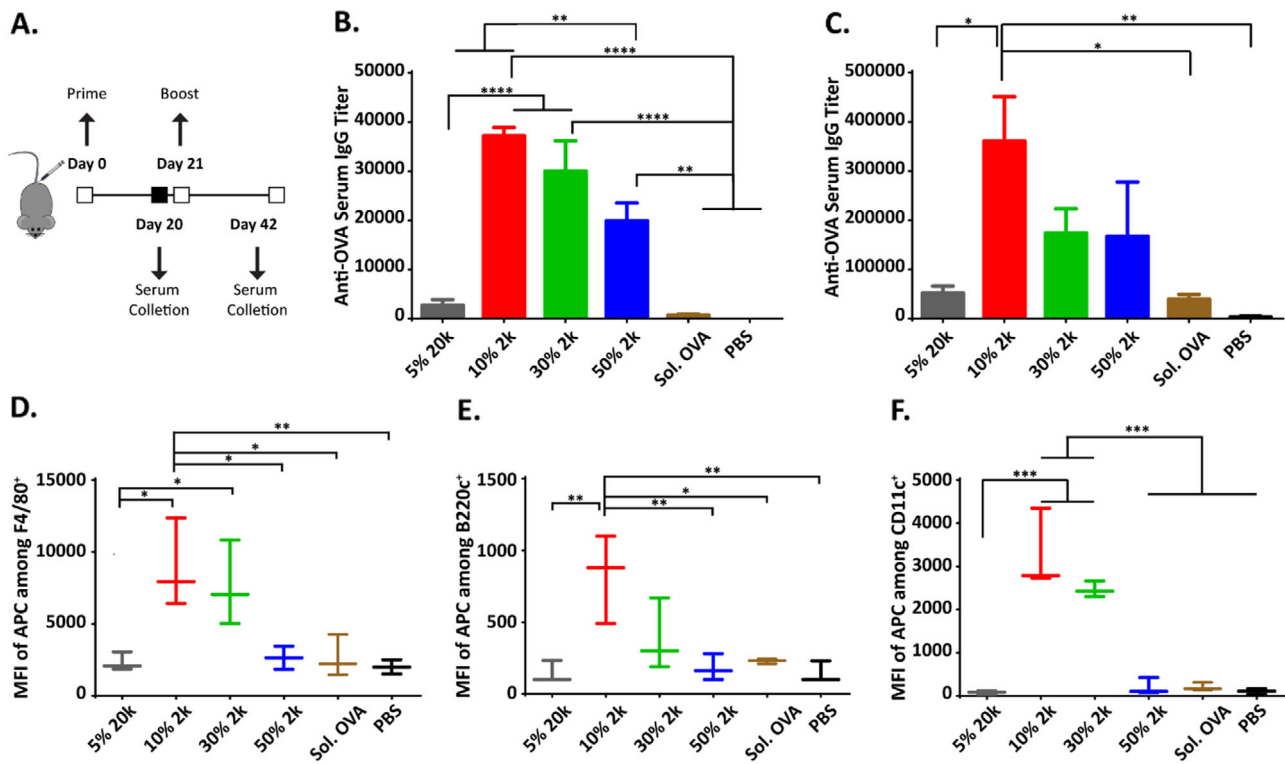


**Figure 3.** Humoral responses elicited by engineered OVA pNPs in immune competent mice: A) Vaccine doses and regimen. Naïve C57BL/6 mice were injected with OVA pNPs and soluble CpG subcutaneously at the tail base on Day 0 (prime immunization) and 21 (boost immunization). Serum anti-OVA IgG titers were measured on B) Day 20 (prime response) and C) Day 28 (boost response). The data were fitted by logarithmic regression. The titer was calculated by solving for the inverse dilution factor resulting in an absorbance value of 0.5. Data represent mean  $\pm$  SEM ( $n = 5$ ). Groups were compared using one-way ANOVA with Tukey's post-test.  $P < 0.05$  was considered statistically different (\* $P < 0.05$ , \*\* $P < 0.01$ , \*\*\* $P < 0.001$ , and \*\*\*\* $P < 0.0001$ ).  $P > 0.05$  was considered not significant. Delivery of pNPs to dLNs: MFI of AlexaFluor 647 associated with OVA NPs among D) F4/80<sup>+</sup> macrophages, E) B220<sup>+</sup> B cells, and F) CD11c<sup>+</sup> DCs obtained from a single cell suspension from draining lymph nodes. Groups were compared using one-way ANOVA with Tukey's post-test.  $P < 0.05$  was considered statistically different (\* $P < 0.05$ , \*\* $P < 0.01$ , \*\*\* $P < 0.005$ ).  $P > 0.05$  was considered not significant.

different particle sizes have been studied with respect to their lymphatic drainage.<sup>[10a,b,42–44,7e,45]</sup> It has been shown that particles exceeding 500 nm can be trapped at the injection site. Nanoparticles smaller than 10 nm, or soluble antigen, diffuse into the lymphatic system easily, but their retention time in the lymph nodes is too short to provide sustained antigen delivery.<sup>[1b]</sup> This may explain why OVA pNPs with 500 nm size and soluble OVA were not delivered to the lymph nodes efficiently, while we observed improved NP uptake by lymph node cells for the smaller OVA pNPs. For smaller pNPs sizes, improved uptake was observed for pNP with lower PEG/OVA ratio.

Encouraged by the fact that OVA pNPs with 10% PEG/OVA ratio resulted in increased OT-I CD8<sup>+</sup> cell proliferation in vitro, improved uptake by APCs (both in vitro and in vivo), and enhanced humoral immune response in vivo, we employed a murine model of B16F10-OVA melanoma to evaluate the therapeutic efficacy of pNPs with a PEG/OVA ratio of 10% compared to solute OVA. Tumor-bearing mice were treated with 10% PEG/OVA pNPs or solute OVA (10  $\mu$ g OVA per 100  $\mu$ L dose), co-administered with CpG (15  $\mu$ g per dose). Following the regimen shown in Figure 4A, we inoculated C57BL/6 mice (10 mice per treatment group) with  $1 \times 10^5$  B16F10-OVA cells in the SC flank on day 0. Treatments with either 10% PEG/OVA pNPs or solute OVA were initiated on day 7 after tumor inoculation. A second treat-

ment was given on day 14. Mice were euthanized after their tumors reached 15 mm in any dimension. Compared to the no treatment control group, mice treated with solute OVA showed slightly better survival. More than 50% of mice treated with solute OVA were euthanized due to large tumor burden on day 20, and 100% of the mice were euthanized on day 21. In contrast, 100% of mice treated with 10% PEG/OVA pNPs were alive on day 21 and showed improved survival until the endpoint of the study (day 24) (Figure 4B). Treatment with 10% PEG/OVA pNPs significantly enhanced antigen-specific CD8<sup>+</sup> T cell immune response compared to solute antigen and PBS groups. (see Figure S3 in the Supporting Information)

The survival rate of B16F10-OVA tumor-bearing mice were increased after immunization with OVA pNPs compared to solute antigen treatment. The survival data observed with OVA pNPs is comparable to previous studies that conducted delivery of OVA antigen in the same B16F10-OVA model.<sup>[46]</sup>

We employed reactive electrospinning, a novel, yet scalable and versatile nanoparticle manufacturing process, for development of engineered OVA pNPs with defined physico-chemical properties. We identified key parameters (e.g., size or PEG/OVA ratio) that determined the immunological responses of pNPs. Specifically, lower PEG/OVA ratios resulted in softer pNPs with larger mesh sizes, which, in turn, resulted in improved CD8<sup>+</sup> T cell

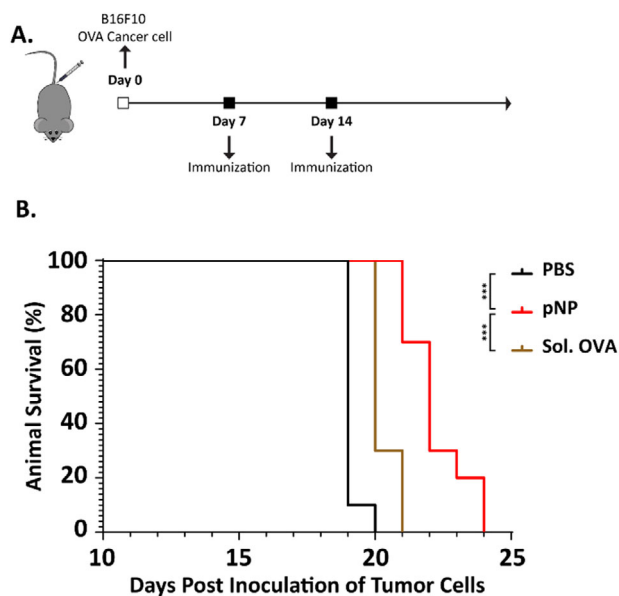


**Figure 4.** Therapeutic effect of engineered OVA pNPs in melanoma-bearing mice: A) Vaccine doses and regimen and B) animal survival. C57BL/6 mice were inoculated subcutaneously with  $1 \times 10^5$  B16F10-OVA cells on day 0. On day 7 and 14, mice were treated with indicated formulations (OVA pNP, soluble OVA, PBS) containing 10  $\mu\text{g}$  per dose OVA and 15  $\mu\text{g}$  per dose CpG (100  $\mu\text{L}$  dose). Data represent mean  $\pm$  SEM ( $n = 10$ ). Groups were compared using Kaplan-Meier estimator analysis.  $P < 0.05$  was considered statistically different (\* $P < 0.05$ , \*\* $P < 0.01$ , and \*\*\* $P < 0.001$ ).  $P > 0.05$  was considered not significant.

activation in vitro and improved lymph node drainage and humoral immune response in vivo. Identifying the significance of these parameters allowed us to design a pNP formulation with preclinical potential. In a preclinical murine model of melanoma, we found that the smaller (200 nm) pNPs of 10% PEG/OVA ratio resulted in improved survival of mice bearing advanced melanoma tumors. In future studies, to improve the clinical relevance, a combination strategy using different types of immunotherapies should be employed. In this case, a combination of OVA pNP administration with adjuvant therapy and immune checkpoint inhibitor therapy could result in further improvement of the preclinical outcomes.

## Experimental Section

**Reagents:** Ovalbumin (OVA), O, O'-bis[2-(N-succinimidylsuccinylamino)ethyl] polyethylene glycol (NHS-PEG-NHS) with a molecular weight of 2000 Da, ethylene glycol, 4,6-diamidino-2-phenylindole dihydrochloride (DAPI), carboxyfluorescein diacetate N-succinimidyl ester (CFSE), Triton-X 100, and tween 20 were used as purchased from Sigma Aldrich, USA. O, O'-bis[2-(N-succinimidylsuccinylamino)ethyl]polyethylene glycol (NHS-PEG-NHS) with a molecular weight of 20 000 Da was purchased from Nanocs Inc., USA. BCA assay, endotoxin removal spin columns, methanol-free formaldehyde, Alexa Flour 488 phalloidin, Alexa Fluor 647 conjugated albumin from bovine serum (BSA), ProLong Gold Antifade Mountant, and 96-well flat bottom immunoplates were purchased from ThermoFisher Scientific, USA. Endotoxin free water was obtained from G- Biosciences, USA. Endotoxin-Free Dulbecco's PBS was purchased from EMD Millipore, USA.

RPMI 1640 media, fetal bovine serum (FBS), penicillin–streptomycin, b-mercaptoethanol, and ACK lysis buffer were obtained from Life Technologies. Granulocyte macrophage-colony-stimulating factor (GM-CSF) was the product of PeproTech, USA. PE/Cy7 anti-mouse CD11c antibody was purchased from Biolegend, USA. Anti-mouse CD8 antibody (CD8 $\alpha$ -APC) was purchased from BD Biosciences, USA. EasySep Mouse CD8+ T Cell Isolation Kit was purchased from STEMCELL Technologies, Canada. Biotinylated Rabbit/goat anti-mouse IgG was purchased from Southern Biotech, USA. Streptavidin-HRP was purchased from R&D Systems, USA. 3,3',5,5'-Tetramethylbenzidine (TMB) substrate was purchased from Surmodics, USA.

**Fabrication of OVA pNPs:** Ovalbumin nanoparticles (OVA pNPs) were prepared using electrospinning. Prior to pNP fabrication, endotoxin-free OVA was prepared using spin columns according to manufacturer's instructions. Protein solutions were prepared by dissolving endotoxin-free ovalbumin (7.5 w/v%) and the desired amount of NHS-PEG-NHS crosslinker (5, 10, 30, or 50 w/w%) in mixtures of endotoxin-free water and ethylene glycol. Water-to-ethylene glycol ratios of 80:20 vol% or 40:60 vol% were used depending on the formulation. OVA/PEG solutions were pumped at a flow rate of 0.1 mL h<sup>-1</sup>. After a droplet had been formed at the outlet of the needle, an electric field was applied which results in formation of the characteristic Taylor cone. After application of  $\approx 10$ –12 kV of voltage, OVA pNPs were electrospun onto a collector sheet (the distance between the needle tip and the collector sheet was adjusted to 20 cm). Afterward, the pNPs were kept at 37 °C for 7 days to complete the crosslinking reaction before being collected in PBS buffer containing 0.01% Tween20. Serial centrifugation was employed to separate the desired nanoparticles from larger particles (see the Supporting Information for detailed centrifugation protocol). Lastly, OVA pNPs were re-dispersed in PBS buffer and stored at 4 °C until further use. The concentration of pNPs was assessed using bicinchoninic acid (BCA) assay according to manufacturer's instructions.

**Characterization of PNP—Scanning Electron Microscopy (SEM):** SEM images were recorded using a FEI Nova 200 Nanolab SEM/FIB at the Michigan Center for Materials Engineering at acceleration voltages of 5 kV. Images were processed using ImageJ (Wayne Rasband, NIH) to obtain the respective nanoparticle size distribution. For particle size determination, > 500 particles per sample were measured using ImageJ.

**Characterization of PNP—Dynamic/Electrophoretic Light Scattering (DLS/ELS):** DLS/ELS measurements were carried out using a Zetasizer Nano ZS (Malvern Panalytical). DLS was employed to measure the particle size distribution in PBS buffer after particle collection. ELS was employed to determine the zeta potential of OVA NPs. 3 individual measurements were carried out per sample and averaged to determine the particle size and zeta potential.

**Characterization of PNP—Atomic Force Microscopy (AFM):** AFM measurements were carried out using an MFP-3D (Oxford Instruments, UK) using CSC-38noAl-A cantilevers (Micromash, USA) with a spring constant of 0.09 N m<sup>-1</sup>. Samples were prepared by electrospinning OVA pNPs directly onto silicon substrates coated with poly(4-Penta fluorophenyl-p-xylylene) via chemical vapor deposition (CVD) polymerization (see the Supporting Information); the substrates were allowed to crosslink at 37 °C for several days prior to use. OVA NPs were localized by scanning the surface in tapping mode over a (5  $\times$  5)  $\mu\text{m}^2$  area and then decreasing the scan area for visualization of a single NP. The force curves were obtained by indenting the tip into the center of an individual nanoparticle and recording the deflection of the cantilever.

**Characterization of PNP—Small Angle Neutron Scattering (SANS):** SANS experiments were carried out at the NIST Center for Neutron Research using the NGB30 instrument. Using neutron wavelength of  $\lambda = 6$  Å and  $\Delta\lambda/\lambda = 0.11$  at detector distances 1.3, 4.0, and 13.2 m, a  $q$ -range of 0.003 to 0.5 Å<sup>-1</sup> was provided. OVA pNPs with PEG/OVA ratio of 10% and 50% dispersed in D<sub>2</sub>O (2 mg mL<sup>-1</sup>) were loaded into 1 mm titanium scattering cells between mounted quartz windows, and a Julabo temperature-controlled bath was used to maintain the sample temperature at 37 °C. SANS data were then collected and reduced using the NCNR IGOR software.<sup>[30]</sup> Data analysis was performed subsequently using the Sasview software.



**Preparation of Bone Marrow-Derived Dendritic Cells (BMDCs):** BMDCs were prepared according to literature protocols.<sup>[31]</sup> C57BL/6 mice were kept in a pathogen-free environment and allowed to acclimate for at least one week before experiments. All animal experiments described in this protocol were compliant with the Committee on Use and Care of Animals (UCUCA) at the University of Michigan and performed according to the established policies and guidelines. Briefly, femur and tibia were harvested from C57BL/6 mice. Bone marrow was flushed with a syringe and collected. The cell suspension was passed through a 40  $\mu\text{m}$  cell strainer. After centrifugation, cells were plated into non-tissue culture treated Petri-dishes at a concentration of 2 million cells per dish in DC media (RPMI 1640 supplemented with 10% FBS, 1% penicillin-streptomycin,  $50 \times 10^{-6}\text{M}$   $\beta$ -mercaptoethanol and  $20 \text{ ng mL}^{-1}$  GM-CSF) at  $37^\circ\text{C}$  with 5%  $\text{CO}_2$ . The media was refreshed on days 3, 6, and 8. BMDCs were used for experiments on days 10–12.

**OVA pNP Uptake by BMDCs:** Internalization of fluorescent OVA pNPs by BMDCs was visualized using confocal microscopy and quantified using flow cytometry. Fluorescent OVA pNPs were obtained by addition of AlexaFluor 647-conjugated albumin from bovine serum (BSA) at  $1 \text{ mg mL}^{-1}$  to the solvent mixture for electrospraying of the nanoparticles. For confocal imaging, BMDCs were seeded on chamber slides ( $10^5$  cells per well) and maintained in a humidified incubator at  $37^\circ\text{C}$  and 5%  $\text{CO}_2$ . Cells were incubated with  $10 \mu\text{g mL}^{-1}$  of OVA NPs for 24 h. The cells were then washed three times with PBS, fixed with 4% paraformaldehyde, washed, and permeabilized with 0.1% Triton-X solution which was followed by treatment with blocking solution of 1% BSA. The actin filaments were stained with AlexaFluor 488-Phalloidin and the nucleus was stained with DAPI. The samples were imaged using a 63x oil-immersion lens on a Nikon A-1 spectral confocal microscope located at the Microscopy and Image Analysis Laboratory (MIL) at the University of Michigan.

Flow cytometry was used for quantitative uptake studies. BMDCs were plated in a 12-well plate at a density of 1 million cells per well in DC media. After 24 h, media was removed from the wells to remove non-adherent cells, and fresh media containing different nanoparticle groups at  $10 \mu\text{g mL}^{-1}$  was added to the wells. After 24-hour incubation of cells with OVA nanoparticles, the cells were washed with PBS three times and then trypsinized. The cells were washed two more times and stained with CD11c-PE/Cy7 and DAPI before analyzing them via flow cytometry using a Cytoflex (Beckman Coulter) cell analyzer located at the Flow Cytometry Core of the University of Michigan. Data were analyzed using FlowJo software.

**CFSE Dilution Assay:** CFSE dilution assay was performed to evaluate the proliferation of OT-I CD8+ cells after co-culture with OVA pNP-treated BMDCs. BMDCs were seeded in 96-well plates at a density of 50 000 cells per well and then incubated with the respective OVA NPs groups, soluble OVA, SIINFEKL (positive control), and PBS (negative control) overnight. Naive CD8+ T cells were isolated from the spleen of OT-I transgenic mice using a magnetic CD8+ T-cell-negative selection kit. OT-I CD8+ cells were fluorescently labeled by incubation with CFSE ( $1 \mu\text{M}$ ) for 10 min at  $37^\circ\text{C}$ . CFSE-labeled OT-I CD8+ T cells were then co-cultured with OVA pNP-treated BMDCs in 96 well plates at a density of 50 000 cells per well for 72 h. BMDCs were washed with PBS three times before co-culture. Cells were then stained with CD8 $\alpha$ -APC and DAPI, and flow cytometry (Cytoflex, Beckman Coulter) was used to determine the percentage of live, proliferated OT-I CD8+ cells. The data was processed using FlowJo software and reported as % CFSE dilution, which was proportional to OT-I CD8+ cell proliferation.

**Immunization:** Six-week-old, female C57BL/6 mice were purchased from Jackson Laboratory. Mice ( $n = 5$  per group) were immunized subcutaneously at the tail base at a dose of  $10 \mu\text{g}$  OVA with  $15 \mu\text{g}$  CpG in  $100 \mu\text{l}$  sterile PBS buffer (primary immunization). Boost immunization was performed on day 21 after primary immunization. On days 20 and 42, blood was collected by submandibular bleed for serum antibody titers analysis. To separate serum, the collected blood was centrifuged at  $10\,000 \times g$  for 5 min. Serum was then stored at  $-80^\circ\text{C}$  until analysis.

**ELISA:** For ELISA analysis, 96 well flat bottom Immunoplates (Thermo Scientific) were coated with  $1 \mu\text{g}$  per well OVA solution in 0.05 M carbonate-bicarbonate buffer (pH 9.6) and incubated overnight at  $4^\circ\text{C}$ .

Plates were then washed with  $50 \times 10^{-3}\text{M}$  Tris, 0.14 M NaCl, 10.05% Tween 20 (pH 8) followed by blocking with  $50 \times 10^{-3}\text{M}$  Tris, 0.14 M NaCl, 1% BSA (pH 8) for 1 h at room temperature. Samples were diluted in  $50 \times 10^{-3}\text{M}$  Tris, 0.14 M NaCl, 0.05% Tween 20, 1% BSA and added to each well for an hour incubation at room temperature. After washing, the plates were incubated with diluted horseradish peroxidase enzyme (HRP) conjugated Rabbit anti-mouse IgG for an hour. The plates were then washed and incubated with TMB substrate solution for 10 min. The reaction was stopped by addition of  $2 \text{ M H}_2\text{SO}_4$  solution. The plates were read at the wavelength of 450 nm using a plate reader.

**Statistical Analysis:** All quantitative experiments were performed in triplicate and are presented as arithmetic mean  $\pm$  SEM. Statistical analysis were performed using SPSS Statistics 24 software. One-way ANOVA with Tukey's post-test was used to determine significance among groups. A  $P$ -value of  $<0.05$  was considered statistically significant ( $*P < 0.05$ ,  $**P < 0.01$ ,  $***P < 0.001$ ;  $****P < 0.0001$ );  $P$ -values of  $>0.05$  were considered not significant (ns).

## Supporting Information

Supporting Information is available from the Wiley Online Library or from the author.

## Acknowledgements

N.H. and S.C. contributed equally to this work. The authors thank the Defense Threat Reduction Agency (DTRA grant #HDTRA1-15-0045) for financial support. Stephanie Christau acknowledges support from the German Science Foundation (DFG) (GZ: CH 1791/1-1). The authors thank the Center for Statistical Consultation and Research (CSCAR) at the University of Michigan for help with statistical analyses. The authors also thank Jonathan Gerszberg, University of Michigan, for preparing substrates for the AFM study. The authors acknowledge the support of the National Institute of Standards and Technology, U.S. Department of Commerce, in providing the neutron research facilities used in this work. Access to NGB30 was provided by the Center for High Resolution Neutron Scattering, a partnership between the National Institute of Standards and Technology and the National Science Foundation under Agreement No. DMR-1508249. The authors thank Elizabeth Kelly at the NIST Center for Neutron Research for technical support. The authors furthermore thank the University of Michigan Center for Materials Characterization for technical support with SEM imaging (NSF grant #DMR-0320740) and the University of Michigan BRCF Flow cytometry core for their technical support (NIH P30CA046592).

## Conflict of Interest

The University of Michigan has filed a patent application (US 62/931512) on materials related to the work described in this manuscript.

## Keywords

B cells, dendritic cells, electrospraying, nanomedicine, ovalbumin, small angle neutron scattering, vaccines

Received: May 4, 2020  
Published online: July 9, 2020

- [1] a) J. J. Moon, B. Huang, D. J. Irvine, *Adv. Mater.* **2012**, *24*, 3724; b) D. J. Irvine, M. A. Swartz, G. L. Szeto, *Nat. Mater.* **2013**, *12*, 978; c) M. S. Goldberg, *Cell* **2015**, *161*, 201.
- [2] P. Sahdev, L. J. Ochyl, J. J. Moon, *Pharm. Res.* **2014**, *31*, 2563.
- [3] C. J. Melief, S. H. Van Der Burg, *Nat. Rev. Cancer* **2008**, *8*, 351.
- [4] Y. Hailemichael, Z. Dai, N. Jaffarzad, Y. Ye, M. A. Medina, X.-F. Huang, S. M. Dorta-Estremera, N. R. Greeley, G. Nitti, W. Peng, *Nat. Med.* **2013**, *19*, 465.
- [5] Y. Fan, J. J. Moon, *Vaccine* **2015**, *3*, 662.
- [6] I. Sagiv-Barfi, D. K. Czerwinski, S. Levy, I. S. Alam, A. T. Mayer, S. S. Gambhir, R. Levy, *Sci. Transl. Med.* **2018**, *10*, eaan4488.
- [7] a) N. M. Molino, M. Neek, J. A. Tucker, E. L. Nelson, S.-W. Wang, *Biomaterials* **2016**, *86*, 83; b) L. Seth, K. M. B. Ferlez, S. A. Kaba, D. M. Musser, S. Emadi, G. R. Matyas, Z. Beck, C. R. Alving, P. Burkhard, D. E. Lanar, *Vaccine* **2017**, *35*, 5448; c) R. Kuai, L. J. Ochyl, K. S. Bahjat, A. Schwendeman, J. J. Moon, *Nat. Mater.* **2017**, *16*, 489; d) B. Choi, H. Moon, S. J. Hong, C. Shin, Y. Do, S. Ryu, S. Kang, *ACS Nano* **2016**, *10*, 7339; e) S. T. Reddy, A. J. Van Der Vlies, E. Simeoni, V. Angeli, G. J. Randolph, C. P. O'Neil, L. K. Lee, M. A. Swartz, J. A. Hubbell, *Nat. Biotechnol.* **2007**, *25*, 1159; f) J. J. Moon, H. Suh, A. Bershteyn, M. T. Stephan, H. Liu, B. Huang, M. Sohail, S. Luo, S. H. Um, H. Khant, *Nat. Mater.* **2011**, *10*, 243; g) I. H. Lee, H. K. Kwon, S. An, D. Kim, S. Kim, M. K. Yu, J. H. Lee, T. S. Lee, S. H. Im, S. Jon, *Angew. Chem.* **2012**, *124*, 8930; h) A. V. Li, J. J. Moon, W. Abraham, H. Suh, J. Elkhader, M. A. Seidman, M. Yen, E.-J. Im, M. H. Foley, D. H. Barouch, *Sci. Transl. Med.* **2013**, *5*, 204ra130; i) L. Jeanbart, M. Ballester, A. De Titta, P. Corthésy, P. Romero, J. A. Hubbell, M. A. Swartz, *Cancer Immunol. Res.* **2014**, *2*, 436; j) Z. Xu, Y. Wang, L. Zhang, L. Huang, *ACS Nano* **2014**, *8*, 3636; k) H. Liu, K. D. Moynihan, Y. Zheng, G. L. Szeto, A. V. Li, B. Huang, D. S. Van Egeren, C. Park, D. J. Irvine, *Nature* **2014**, *507*, 519; l) R. A. Rosalia, L. J. Cruz, S. van Duikeren, A. T. Tromp, A. L. Silva, W. Jiskoot, T. de Gruijl, C. Löwik, J. Oostendorp, S. H. van der Burg, *Biomaterials* **2015**, *40*, 88; m) Y.-C. Chiu, J. M. Gammon, J. I. Andorko, L. H. Tostanoski, C. M. Jewell, *ACS Biomater. Sci. Eng.* **2015**, *1*, 1200; n) P. Lizotte, A. Wen, M. Sheen, J. Fields, P. Rojanasopondist, N. Steinmetz, S. Fiering, *Nat. Nanotechnol.* **2016**, *11*, 295.
- [8] a) A. E. Gregory, R. Titball, D. Williamson, *Front. Cell. Infect. Microbiol.* **2013**, *3*; b) M. Singh, *Vaccine Adjuvants and Delivery Systems*, John Wiley & Sons, New York **2007**; c) L. Liu, P. Ma, H. Wang, C. Zhang, H. Sun, C. Wang, C. Song, X. Leng, D. Kong, G. Ma, *J. Controlled Release* **2016**, *225*, 230.
- [9] a) V. Torchilin, *Drug Discovery Today: Technol.* **2008**, *5*, 95; b) Y. Lu, W. Sun, Z. Gu, *J. Controlled Release* **2014**, *194*, 1; c) E. A. Simone, T. D. Dziubla, F. Colon-Gonzalez, D. E. Discher, V. R. Muzykantov, *Biomacromolecules* **2007**, *8*, 3914; d) K. Dutta, D. Hu, B. Zhao, A. E. Ribbe, J. Zhuang, S. Thayumanavan, *J. Am. Chem. Soc.* **2017**, *139*, 5676; e) C. Cai, S. Mao, T. Kissel, *Asian J. Pharm. Sci.* **2016**, *11*, 64.
- [10] a) S. D. Xiang, A. Scholzen, G. Minigo, C. David, V. Apostolopoulos, P. L. Mottram, M. Plebanski, *Methods* **2006**, *40*, 1; b) A. Stano, C. Nembrini, M. A. Swartz, J. A. Hubbell, E. Simeoni, *Vaccine* **2012**, *30*, 7541; c) P. L. Mottram, D. Leong, B. Crimeen-Irwin, S. Gloster, S. D. Xiang, J. Meanger, R. Ghildyal, N. Vardaxis, M. Plebanski, *Mol. Pharmaceutics* **2007**, *4*, 73.
- [11] a) S. Kumar, A. C. Anselmo, A. Banerjee, M. Zakrewsky, S. Mitragotri, *J. Controlled Release* **2015**, *220*, 141; b) C. A. Vaine, M. K. Patel, J. Zhu, E. Lee, R. W. Finberg, R. C. Hayward, E. A. Kurt-Jones, *J. Immunol.* **2013**, *190*, 3525.
- [12] S. Neumann, K. Burkert, R. Kemp, T. Rades, P. R. Dunbar, S. Hook, *Immunol. Cell Biol.* **2014**, *92*, 535.
- [13] B. S. Zolnik, A. Gonzalez-Fernandez, N. Sadrieh, M. A. Dobrovolskaia, *Endocrinology* **2010**, *151*, 458.
- [14] a) S. Burgdorf, M. Embgenbroich, *Front. Immunol.* **2018**, *9*, 1643; b) O. P. Joffre, E. Segura, A. Savina, S. Amigorena, *Nat. Rev. Immunol.* **2012**, *12*, 557.
- [15] B. Slütter, L. Plapied, V. Fievez, M. A. Sande, A. des Rieux, Y.-J. Schneider, E. Van Riet, W. Jiskoot, V. Pr eat, *J. Controlled Release* **2009**, *138*, 113.
- [16] L. J. Cruz, P. J. Tacken, I. S. Zeelenberg, M. Srinivas, F. Bonetto, B. Weigelin, C. Eich, I. J. de Vries, C. G. Figdor, *Mol. Pharmaceutics* **2014**, *11*, 4299.
- [17] a) S. Hirotsue, I. C. Kourtis, A. J. van der Vlies, J. A. Hubbell, M. A. Swartz, *Vaccine* **2010**, *28*, 7897; b) J. T. Wilson, S. Keller, M. J. Manganiello, C. Cheng, C.-C. Lee, C. Opara, A. Convertine, P. S. Stayton, *ACS Nano* **2013**, *7*, 3912.
- [18] a) V. Hornung, F. Bauernfeind, A. Halle, E. O. Samstad, H. Kono, K. L. Rock, K. A. Fitzgerald, E. Latz, *Nat. Immunol.* **2008**, *9*, 847; b) H. Li, S. B. Willingham, J. P.-Y. Ting, F. Re, *J. Immunol.* **2008**, *181*, 17; c) F. A. Sharp, D. Ruane, B. Claass, E. Creagh, J. Harris, P. Malyala, M. Singh, D. T. O'Hagan, V. P etrilli, J. Tschopp, *Proc. Natl. Acad. Sci. USA* **2009**, *106*, 870.
- [19] L. Zhao, A. Seth, N. Wibowo, C.-X. Zhao, N. Mitter, C. Yu, A. P. Middelberg, *Vaccine* **2014**, *32*, 327.
- [20] a) M. Kanekiyo, C.-J. Wei, H. M. Yassine, P. M. McTamney, J. C. Boyington, J. R. Whittle, S. S. Rao, W.-P. Kong, L. Wang, G. J. Nabel, *Nature* **2013**, *499*, 102; b) L. Deng, T. Mohan, T. Z. Chang, G. X. Gonzalez, Y. Wang, Y.-M. Kwon, S.-M. Kang, R. W. Compans, J. A. Champion, B.-Z. Wang, *Nat. Commun.* **2018**, *9*, 359; c) Y. Jang, W. T. Choi, W. T. Heller, Z. Ke, E. R. Wright, J. A. Champion, *Small* **2017**, *13*, 1700399; d) T. Z. Chang, I. Diambou, J. R. Kim, B. Wang, J. A. Champion, *Bioeng. Transl. Med.* **2017**, *2*, 120; e) S. I. Lim, C. I. Lukianov, J. A. Champion, *J. Controlled Release* **2017**, *249*, 1; f) L. H. Estrada, J. Champion, *Biomater. Sci.* **2015**, *3*, 787; g) G. S. Shukla, Y.-J. Sun, S. C. Pero, G. S. Sholler, D. N. Krag, *J. Immunol. Methods* **2018**, *460*, 51.
- [21] D. M. Da Silva, D. V. Pastrana, J. T. Schiller, W. M. Kast, *Virology* **2001**, *290*, 350.
- [22] A. N. Tsoras, J. A. Champion, *Annu. Rev. Chem. Biomol. Eng.* **2019**, *10*, 337.
- [23] a) X. Dong, J. Liang, A. Yang, C. Wang, D. Kong, F. Lv, *ACS Appl. Mater. Interfaces* **2018**, *10*, 21861; b) X. Dong, Z. Sun, J. Liang, H. Wang, D. Zhu, X. Leng, C. Wang, D. Kong, F. Lv, *Nanomedicine* **2018**, *14*, 1087; c) Z. Sun, J. Liang, X. Dong, C. Wang, D. Kong, F. Lv, *ACS Appl. Mater. Interfaces* **2018**, *10*, 20315; d) K. T. Gause, Y. Yan, N. M. O'Brien-Simpson, J. Cui, J. C. Lenzo, E. C. Reynolds, F. Caruso, *Adv. Funct. Mater.* **2016**, *26*, 7526; e) K. T. Gause, Y. Yan, J. Cui, N. M. O'Brien-Simpson, J. C. Lenzo, E. C. Reynolds, F. Caruso, *ACS Nano* **2015**, *9*, 2433; f) A. N. Tsoras, J. A. Champion, *Bioconjugate Chem.* **2018**, *29*, 776; g) T. Z. Chang, S. S. Stadtmiller, E. Staskevicius, J. A. Champion, *Biomater. Sci.* **2017**, *5*, 223.
- [24] A. Jaworek, A. T. Sobczyk, *J. Electrostat.* **2008**, *66*, 197.
- [25] Y. Wu, J. A. MacKay, J. R. McDaniel, A. Chilkoti, R. L. Clark, *Biomacromolecules* **2008**, *10*, 19.
- [26] A. Gomez, D. Bingham, L. De Juan, K. Tang, *J. Aerosol Sci.* **1998**, *29*, 561.
- [27] A. Jaworek, *Powder Technol.* **2007**, *176*, 18.
- [28] J. W. Myerson, P. N. Patel, N. Habibi, L. R. Walsh, Y.-W. Lee, D. C. Luther, L. T. Ferguson, M. H. Zaleski, M. E. Zamora, O. A. Marcos-Contreras, P. M. Glassman, I. Johnston, E. D. Hood, T. Shuvaeva, J. V. Gregory, R. Y. Kiseleva, J. Nong, K. M. Rubey, C. F. Greineder, S. Mitragotri, G. S. Worthen, V. M. Rotello, J. Lahann, V. R. Muzykantov, J. S. Brenner, *bioRxiv* **2020**, <https://doi.org/10.1101/2020.04.15.037564>.
- [29] N. Habibi, D. F. Quevedo, J. V. Gregory, J. Lahann, *Wiley Interdiscip. Rev.: Nanomed. Nanobiotechnol.* **2020**, *12*, e1625.
- [30] S. R. Kline, *J. Appl. Crystallogr.* **2006**, *39*, 895.
- [31] M. B. Lutz, N. Kukutsch, A. L. Ogilvie, S. R oßner, F. Koch, N. Romani, G. Schuler, *J. Immunol. Methods* **1999**, *223*, 77.
- [32] S. Rahmani, S. Ashraf, R. Hartmann, A. F. Dishman, M. V. Zyuzin, K. Chris, W. J. Parak, J. Lahann, *Bioeng. Transl. Med.* **2016**, *1*, 82.

- [33] R. García, I. B. Recalde, J. E. Figueruelo, A. Campos, *Macromol. Chem. Phys.* **2001**, *202*, 3352.
- [34] P. Malo de Molina, S. Lad, M. E. Helgeson, *Macromolecules* **2015**, *48*, 5402.
- [35] G. Porod, *Colloid Polym. Sci.* **1951**, *124*, 83.
- [36] P. Debye, H. Anderson Jr, H. Brumberger, *J. Appl. Phys.* **1957**, *28*, 679.
- [37] A. L. Weisenhorn, M. Khorsandi, S. Kasas, V. Gotzos, H.-J. Butt, *Nanotechnology* **1993**, *4*, 106.
- [38] S. Ohya, S. Kidoaki, T. Matsuda, *Biomaterials* **2005**, *26*, 3105.
- [39] J. Cui, R. De Rose, J. P. Best, A. P. Johnston, S. Alcantara, K. Liang, G. K. Such, S. J. Kent, F. Caruso, *Adv. Mater.* **2013**, *25*, 3468.
- [40] P. J. Flory, *Polymer* **1979**, *20*, 1317.
- [41] X. Banquy, F. Suarez, A. Argaw, J.-M. Rabanel, P. Grutter, J.-F. Bouchard, P. Hildgen, S. Giasson, *Soft Matter* **2009**, *5*, 3984.
- [42] K. K. Tran, H. Shen, *Biomaterials* **2009**, *30*, 1356.
- [43] J. M. Brewer, K. G. Pollock, L. Tetley, D. G. Russell, *J. Immunol.* **2004**, *173*, 6143.
- [44] T. Fife, A. Gamvrellis, B. Crimeen-Irwin, G. A. Pietersz, J. Li, P. L. Mottram, I. F. McKenzie, M. Plebanski, *J. Immunol.* **2004**, *173*, 3148.
- [45] V. Manolova, A. Flace, M. Bauer, K. Schwarz, P. Saudan, M. F. Bachmann, *Eur. J. Immunol.* **2008**, *38*, 1404.
- [46] a) H. Kim, D. Sehgal, T. A. Kucaba, D. M. Ferguson, T. S. Griffith, J. Panyam, *Nanoscale* **2018**, *10*, 20851; b) M. Jambhrunkar, Y. Yang, M. Yu, M. Zhang, P. Abbaraju, T. Ghosh, M. Kalantari, Y. Wang, N. McMillan, C. Yu, *Mater. Today Adv.* **2020**, *6*, 100069; c) H. A. Hassan, L. Smyth, J. T.-W. Wang, P. M. Costa, K. Ratnasothy, S. S. Diebold, G. Lombardi, K. T. Al-Jamal, *Biomaterials* **2016**, *104*, 310; d) S.-Y. Kim, S. Kim, J.-E. Kim, S. N. Lee, I. W. Shin, H. S. Shin, S. M. Jin, Y.-W. Noh, Y. J. Kang, Y. S. Kim, *ACS Nano* **2019**, *13*, 12671; e) S. Kos, A. Lopes, V. Preat, M. Cemazar, U. L. Tratar, B. Ucakar, K. Vanvarenberg, G. Sersa, G. Vandermeulen, *PLoS One* **2019**, *14*.